Meteorol. Z. (Contrib. Atm. Sci.), Early Access DOI 10.1127/metz/2023/1202

Lifetime nowcasting of thunderstorms over Germany using a multi-source data-based fuzzy-logic approach

Isabella Zöbisch[1*], Tobias Zinner[2] and Kathrin Wapler[3]

[1]Deutsches Zentrum für Luft- und Raumfahrt, Institut für Physik der Atmosphäre, Oberpfaffenhofen, Germany
[2]Meteorologisches Institut, Ludwig-Maximilians-Universität München, Munich, Germany
[3]Deutscher Wetterdienst, Offenbach, Germany

(Manuscript received May 31, 2023; in revised form August 2, 2023; accepted August 17, 2023)

Abstract

Due to technical progress in sensor technology and computer power, observation and model data are operationally available today with a high spatial and temporal resolution, suitable for thunderstorm detection and prediction. However, nowcasting the remaining lifetime of an observed thunderstorm is still a challenge to date. To improve nowcasting of deep convective cells, we developed the algorithm LOC-lifetime that predicts the remaining lifetime of thunderstorms based on life-cycle signatures present in satellite, radar, lightning and numerical weather prediction model data. We use the mathematical method "fuzzy logic" to combine this multi-source input and to categorize the thunderstorm evolution into the life-cycle sets *growth* and *decay*. We analyzed a data set of almost 1,800 thunderstorms that occurred during the summer months June 2016, May, June, July 2017 and June 2018. The data reveal highly variable life cycles which make it difficult to predict the remaining lifetime on basis of life-cycle statistics. Nevertheless, LOC-lifetime offers an improved nowcasting quality compared to a simpler nowcasting method as it increases the probability of correct prediction and reduces the root-mean-square error. Therefore, we propose the lifetime prediction via LOC-lifetime as a useful tool in combination with other existing algorithms to nowcast and forecast thunderstorms.

Keywords: thunderstorms, Germany, nowcasting, multi-source, fuzzy logic

1 Introduction

Lightning, hail, turbulence and heavy rain are only four examples of dangerous weather phenomena associated with thunderstorms having high impact on society and safety (Brooks and Dotzek, 2008). For example, aviation is especially affected by thunderstorms as they can cause, e.g., icing of air plane turbines in the upper troposphere consequently lead to malfunction (Tafferner et al., 2008). Thunderstorm nowcasting can be used today to optimize flight routes which results in reduced delays, fuel savings and higher safety (Forster et al., 2016). Since heavy thunderstorms will become more frequent due to climate change (Sander, 2011; Rädler et al., 2019), an improved nowcasting is gaining relevance.

Besides the prediction of the onset of convection, also nowcasting the remaining lifetime of an already existing and observed thunderstorm may add a useful feature to thunderstorm prediction in general. Here, we present the structure and work flow of our new nowcasting algorithm, named LOC-lifetime (Life cycle Of deep Convection based lifetime nowcasting), that predicts the remaining lifetime of detected thunderstorm cells.

*Corresponding author: Isabella Zöbisch, Deutsches Zentrum für Luft- und Raumfahrt, Institut für Physik der Atmosphäre, Münchener Str. 20, 82234 Weßling, Germany, e-mail: isabella.zoebisch@dlr.de

Most nowcasting methods today do not consider the stage of development of a thunderstorm or use the information on life cycle characteristics. However, a variety of thunderstorm nowcasting algorithms exist using single or multi data input for various methods to predict the future size, position, development and/or intensity of a thunderstorm (e.g., Wilson et al., 1998; Mueller et al., 2003; Roberts and Rutledge, 2003; Zinner et al., 2008; Hering et al., 2015; Goyal et al., 2017; Leinonen et al., 2022). In case nowcasting is based on only one data source, mainly satellite (e.g., Zinner et al., 2013; Goyal et al., 2017) or radar data (e.g., Kober and Tafferner, 2009; Hering et al., 2015) are used. For example, Zinner et al. (2008) use satellite data to detect, track and nowcast thunderstorms based on a pyramidal image matcher for lead times up to 60 min. Goyal et al. (2017) predict cloud top brightness temperatures for lead times up to 180 min via extrapolation techniques on basis of satellite data. Kober and Tafferner (2009) predict thunderstorms up to 60 min on basis of radar data with the same method of the pyramidal image matcher as in Zinner et al. (2008) and showed that extrapolation techniques based on a pyramidal image matcher outperform extrapolations based on persistence. A prediction algorithm that is based on a combination of different data sources is, for example the Auto-Nowcast System ANC (Mueller et al., 2003). In this approach, fuzzy logic is used to combine

radar, satellite, sounding, mesonet, profiler and numerical boundary layer data in addition to forecaster input. The approach outperforms extrapolation and persistence of lead times up to 60 min. Roberts and Rutledge (2003) used satellite data in addition to radar data to increase the lead time and accuracy of the nowcasting of convective storm initiation and growth compared to nowcasts based on radar data alone. James et al. (2018) tracked and nowcasted thunderstorms up to 60 min by combining radar products, lightning observations and numerical weather prediction (NWP) model data and improved the quality of warnings for severe convective weather events (NowCastMIX) in this way. Cintineo et al. (2018) developed Probsevere LightningCast, an algorithm that predicts the next hour lightning activity using satellite data and a deep learning approach to provide early alerts for developing hazardous conditions. Leinonen et al. (2022) designed a machine learning approach based on radar, satellite, lighting, NWP and digital elevation model data to predict lightning, hail and heavy rain up to 60 min. They showed that lightning prediction is robust to at least 60 min.

The prediction of thunderstorms is a well known challenge due to complex interactions of dynamics and microphysics during their life cycle. Most of the presented nowcasting tools were developed to predict the convective initiation of thunderstorms or their severity, in addition to their movement and/or local displacement. No explicit lifetime nowcasting has been done yet, although the information of the remaining lifetime of a thunderstorm would be helpful for many applications, e.g., flight route planing with regard to higher safety and fuel savings. In this study, we combine information on thunderstorm life-cycle characteristics from observational and model output sources as revealed in Zöbisch et al. (2020) and a fuzzy-logic approach to predict remaining lifetimes after detection.

Many studies analyze life-cycle characteristics in different data sources such as satellite, radar, lightning or NWP model data. Thus, characteristic signatures were revealed for the life cycle stages. For instance, a growing thunderstorm is characterized by an increasing optical thickness and an increasing cloud top height (Roberts and Rutledge, 2003; Mecikalski et al., 2011; Zöbisch et al., 2020). The lightning activity intensifies until it reaches its maximum during the maturity stage (Rigo et al., 2010; Mattos and Machado, 2011; Jurkovik et al., 2015). During decay, the updraft intensity is reduced until its supply diminishes (Byers and Braham Jr., 1948). Other studies analyzed the correlation of the thunderstorm lifetime with certain observational parameters, showing that the lifetime correlates positively with the coverage area (e.g., Machado et al., 1997; Mathon and Laurent, 2001; Feng et al., 2012), the thunderstorm maximum reflectivity (e.g., Davini et al., 2012; Zöbisch et al., 2020) and the lightning occurrence (e.g., Rigo et al., 2010; Wapler, 2021).

The thunderstorm definition and the detection method, used for this study, are presented in Section 2. The data sources and used parameters are described in Section 3. The fuzzy-logic based nowcasting algorithm LOC-lifetime is presented in a case study in Section 4. We verify the nowcasting algorithm via cross-validation in Section 5. For the purpose of validation, a simpler nowcasting method is designed to evaluate the gain in nowcasting quality. At the end, results are summarized and discussed (Section 6).

2 Thunderstorm definition

We define a thunderstorm as a deep moist convective region. To locate these regions we use the algorithm Cb-TRAM (Zinner et al., 2008; Zinner et al., 2013) which detects, tracks and nowcasts convective objects in satellite data. Cb-TRAM distinguishes between three convection categories: *early development, rapid development* and *maturity*. *Early development* is described by a strong vertical and/or horizontal growth in the lower troposphere indicated by a rapid cooling visible in the IR10.8 channel and an intensifying reflectivity signal in the HRV channel. *Rapid development* is detected in case of strong cooling in the upper troposphere (WV6.2). *Maturity* is represented by a specific difference between the WV6.2 and IR10.8 channels indicating a high cloud top connected with moisture close to or already in the stratosphere, in addition to a turbulent appearance of the cloud top (e.g. overshooting top; visible in a strong texture in HRV – day times or WV6.2 – night times). To exclude thin cirrus, the difference between T10.8 and T12.0 is used. In this study we define the thunderstorm lifetime as the period of Cb-TRAM detections. Further, we consider only life cycles with at least one maturity time step.

One advantage of thunderstorm detection using satellite data is that already convective initiation can be detected. However, this is only possible in an environment without overlaying clouds. When the developing thunderstorm in the lower troposphere is covered by (cirrus) clouds at higher levels, the convective cell will be detected only after its top has punched through the surrounding cirrus shield.

The thunderstorm detection via Cb-TRAM is exemplarily presented in Figure 1. It shows a Cb-TRAM detection of a relatively isolated stationary thunderstorm cell ‘1315’ over the Breisgau region (Southwestern Germany) on the 17th of June 2016. This thunderstorm cell is detected for 90 min (12:23–13:48 UTC) in 5-min intervals. At the first detection step, it is categorized as a rapid developing cell (orange) since its cloud top is already relatively high (at 8 km height, not shown). As seen one time step before (12:18 UTC), cloudiness can already be identified in this region, however, the thresholds for a detection via Cb-TRAM are not reached yet.

After the thunderstorm is detected as *rapid development* for four time steps (20 min), the next three time steps (15 min) are categorized as *early development* (yellow). Hence, the specific thresholds for an

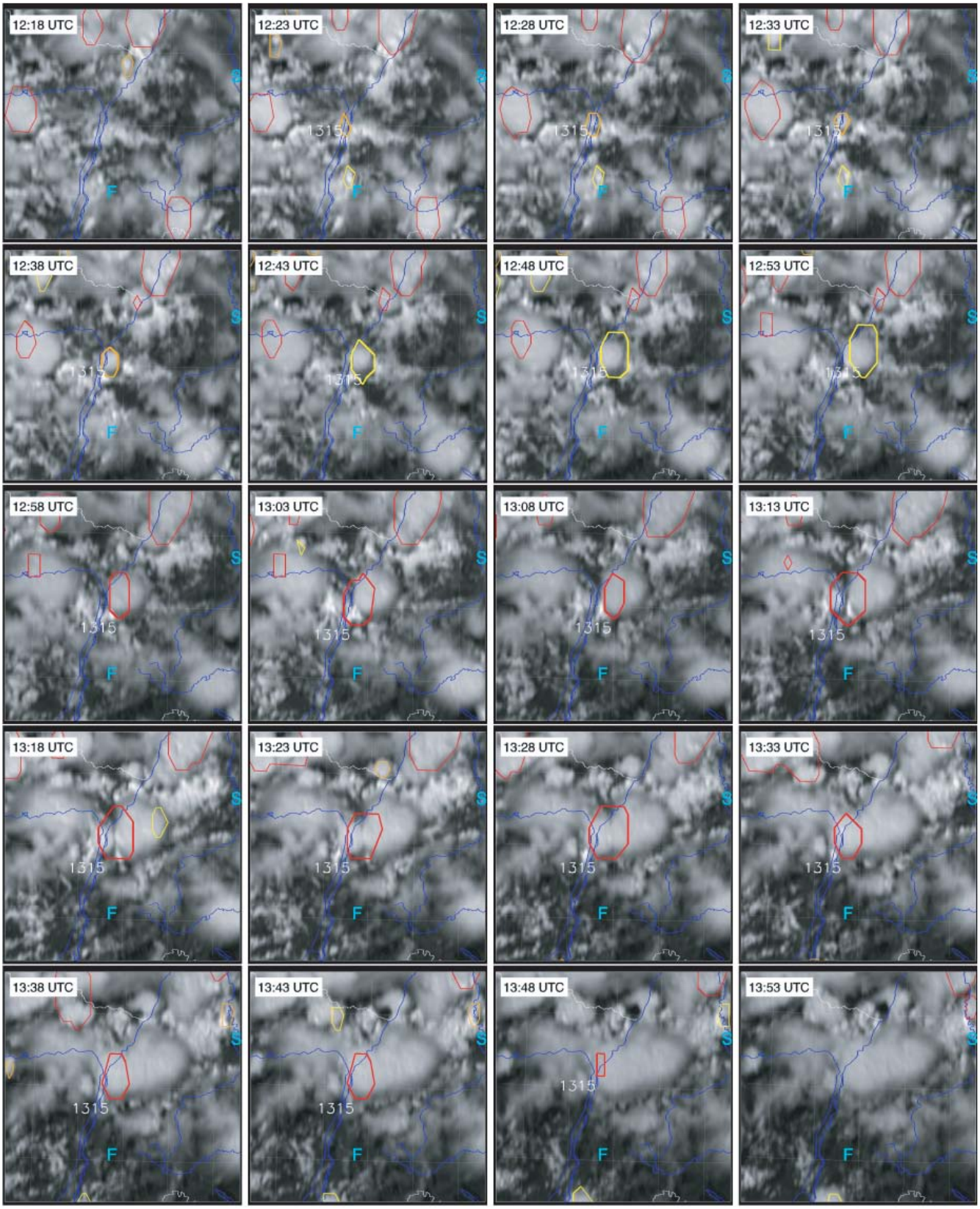

Figure 1: 180 × 180 km detail of a satellite HRV channel and the corresponding detection via Cb-TRAM of the thunderstorm cell "1315" (no parallax correction) over the Breisgau region (Southwestern Germany) on the 17th of June 2016. The thunderstorm cell is detected for 90 min every 5 min (12:23–13:48 UTC). The colors yellow, orange and red represent the convection categories *early development, rapid development* and *maturity*. The turquoise letters "F" and "S" show the locations of the cities Freiburg and Stuttgart.

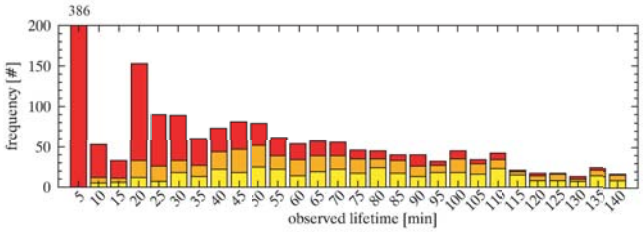

Figure 2: Lifetime frequency distribution of thunderstorms with lifetimes between 5 and 140 min that occurred over Germany during the months June 2016, May, June and July 2017 and June 2018. The colors yellow, orange and red indicate the proportion of the convection categories *early development, rapid development* and *maturity* which the thunderstorm showed at the first detection step.

early development are reached here. After 35 min detection (12:58), the thunderstorm reaches the relevant thresholds for *maturity* (red) for the first time. A cirrus shield developing eastwards of the thunderstorm object is not part of the thunderstorm detection. During the last 20 min of the thunderstorms lifetime, the area decreases – probably due to a weakening updraft, until it diminishes completely and the thunderstorm detection ends. Although the thunderstorm detection ends, its high cirrus shield – the anvil – exists further (13:53 UTC). As we use Cb-TRAM, we focus on the detection of regions with deep moist convection including strong updrafts, that are most dangerous and for instance highly relevant for aircraft safety.

In this study, we consider almost 1,800 thunderstorms that occurred over Germany during the summer months June 2016 (700 thunderstorms), Mai (213), June (189), July 2017 (311) and June 2018 (345). The lifetime frequency distribution of all considered thunderstorms with lifetimes between 5 and 140 min is presented in Figure 2. Additionally, the information of the convection stage detected via Cb-TRAM at the first detection step (colors) is shown. The development stage at the first detection indicates if convective initiation (yellow), rapid growth (orange) or mature (red) is detected. A mature event at the first detection indicates that the beginning of the life cycle is missed due to, e.g., overlaying clouds resulting in a first detection of an already well-developed thunderstorm. In general, the frequency of thunderstorms decreases with an increasing lifetime.

The figure reveals that longer lifetimes contain less well-developed thunderstorms (red) at the first detection, as well in absolute numbers as in relative share. We identify a high number of thunderstorms with lifetimes of 5 min containing only mature developments. Thunderstorms with 10 and 15 min also show mainly mature development at the first detection, contrary to other short lifetimes, they are strikingly rare.

Most likely, very short lifetimes represent incomplete life cycles. A manual evaluation reveals that in case of 10 and 15 min lifetimes, the detection of a well-developed thunderstorm mostly ends rapidly due to a merging event. As a consequence, we assume that the decay of most of these short-lived thunderstorms is not detected. Also, short lifetimes often contain incomplete life cycles with regard to the beginning of their life cycle. We assume that the early development is missed due to, e.g., splitting events or higher cloud cover impeding a satellite-based detection. Correspondingly, long observed lifetimes are more likely to contain early development stages. We conclude that it is more likely to find complete life cycles only among the longer lifetimes in our data set.

3 Data sources

Parameters from satellite, radar, lightning detection and NWP model are considered in LOC-lifetime. In Zöbisch et al. (2020), several parameters are analyzed by means of potential skill for nowcasting thunderstorms. There a parameter is defined as one with an appropriate nowcasting skill for the lifetime prediction, if it indicates the actual life cycle stage and/or the total lifetime (short or long) of the detected thunderstorm. The resulting relevant parameters are presented in Table 1 and described briefly here. They are introduced in detail in Zöbisch et al. (2020).

3.1 Geostationary satellite

We use satellite parameters from the geostationary Meteosat Second Generation satellite (MSG, Schmetz et al., 2002) with a temporal resolution of 5 min and a spatial resolution of 3×3 km at the sub-satellite point. We use the parameters minimum Brightness Temperature (BT_{min}), minimum cloud optical thickness (τ_{min}) and Area of the Cb-TRAM cell (A_{cb}) for the lifetime nowcasting as a measure of the vertical and horizontal extent of the thunderstorm object. On basis of the visible and infrared channels, the parameters Brightness Temperature (BT) and cloud optical thickness (τ) are calculated via the "Algorithm for the Physical Investigation of Clouds with SEVIRI" (APICS, Bugliaro et al., 2011) and the "cirrus optical properties derived from CALIOP and SEVIRI algorithm during day and night" algorithm (COCS, Kox et al., 2014). The parameters BT_{min} and τ_{min} represent the mean of the pixels with the lowest 10 % of BT inside the thunderstorm object as detected by Cb-TRAM to focus on the most active regions. The parameter A_{cb} describes the horizontal extent of the detected thunderstorm object. As presented in Zöbisch et al. (2020) the parameter BT_{min} shows high values at the beginning of long-lived thunderstorms and a distinctive decrease during growth. Therefore, the absolute values and temporal changes of BT_{min} are considered in the lifetime prediction. Since the parameters τ_{min} and A_{cb} show prominent temporal evolution in the beginning and end (sharp in- and decrease) of the life cycle, LOC-lifetime considers the temporal variations.

Table 1: Parameters used for lifetime nowcasting with LOC-lifetime. The letters 'a' and 't' indicate whether the absolute value and/or the temporal change over 5 min of the parameters are used for nowcasting.

source	parameter	abbrev.	unit	a, t
MSG	minimum Brightness Temperature	$BT_{\min}$	K	a, t
	minimum cloud optical thickness	$\tau_{\min}$	–	t
	Area of the Cb-TRAM cell	A_{cb}	km^2	t
Radar	maximum Vertically Integrated Liquid water	$VIL_{\max}$	$\mathrm{kg\,m}^{-2}$	a, t
LINET	Lightning detection during 5 min	Li	$\#\,5\,\mathrm{min}^{-1}$	t
COSMO	maximum Convective Available Potential Energy	$CAPE_{\max}$	$\mathrm{J\,kg}^{-1}$	a
	Relative Humidity at 700 hPa	RH	%	a

3.2 Ground-based radar

We also use the 3D radar product Vertically Integrated Liquid water (*VIL*) provided by the DWD (German Meteorological Service). The parameter *VIL* is calculated with data from the volume scan of the polarimetric doppler C-band radar system operated by the DWD. The volume scan of each of the 17 radar systems of the DWD network is available ever 5 min with a horizontal radius of up to 180 km and a vertical extent of 10 km. The calculation of *VIL* is described in Greene and Clark (1972). The parameter maximum Vertically Integrated Liquid water ($VIL_{\max}$) represents the mean of the 10 % pixels with the highest *VIL* values inside the thunderstorm object to focus on the most convective region and reduce the influence of outliers. The life cycle analyses in Zöbisch et al. (2020) showed a distinctive increase at the life cycle beginning and a decrease during the decay for long-lived thunderstorms as well as a positive correlation between absolute values and lifetimes. Therefore, absolute values and the temporal variations of $VIL_{\max}$ are used in LOC-lifetime.

3.3 Ground-based lightning

Lightning data are provided from the nowcast GmbH which operates the "European ground-based LIghtning NETwork" (LINET, Betz et al., 2009) that is based on the very low frequency (3–30 kHz) and low (30–300 kHz) lightning detection technique. The parameter Lightning detection during 5 min (*Li*) used in LOC-lifetime that represents the sum of lightning detections that occurred inside the thunderstorm cell up to 5 min before each detection. Since the life cycle study showed that the lightning activity of long-lived thunderstorms increases/decreases strongly during the growth/decay phase, the temporal variation of *Li* is used for the lifetime nowcasting.

3.4 NWP model

Parameters from the Consortium for Small-Scale Modeling (COSMO) model operated at the DWD (Baldauf et al., 2006) are used in LOC-lifetime to describe the environmental conditions. In May 2018, the COSMO-DE model was replaced by COSMO-D2. The COSMO-DE/-D2 model has a spatial resolution of 2.8/2.2 km and is separated vertically into 50/65 model layers. Forecasts are updated every 3 hours and available with an interval of 1 hour until 21 hours. The latest available forecast is used for the nowcasting. The hourly output from COSMO is interpolated to a 5 min resolution similar to the temporal resolution of the observational data. The model parameter information inside a box of 50 km radius around the thunderstorm object (hereinafter referred to as: enlarged thunderstorm object) is considered to minimize the effect of an incidentally matching modelled thunderstorm (which would completely change the environmental conditions). The mean of 10 % pixels with highest Convective Available Potential Energy (*CAPE*) values inside the enlarged thunderstorm object is calculated for the parameter maximum Convective Available Potential Energy ($CAPE_{\max}$) to focus on the highest potential of thunderstorm development and to reduce outliers. The mean of all pixels inside the enlarged thunderstorm cell is calculated for the parameter Relative Humidity at 700 hPa (*RH*). The predictable skill of $CAPE_{\max}$ and *RH* has been analyzed and confirmed by several studies (Kuligowski and Barros, 1998; Kaltenböck et al., 2009; Kahraman et al., 2017). Accordingly, the life cycle study Zöbisch et al. (2020) reveals that long-lived thunderstorms are likely to contain high/low $CAPE_{\max}$/*RH* values. Consequently, the absolute values of the model parameters are used for the nowcasting with LOC-lifetime.

4 Nowcasting method

The fuzzy-logic-based nowcasting algorithm LOC-lifetime is developed to predict the remaining lifetime of detected thunderstorm cells. The method fuzzy logic, which was introduced by Zadeh (1965), is well established in weather prediction and used, for example, for marine forecasting (Hansen, 1997), forecasting temperature and icing on streets (Hertl and Schaffar, 1998), forecasting cloud top ceiling height and horizontal visibility at airports (Hansen, 2007), as well as for nowcasting convective initiation (Stich, 2013) and future thunderstorm occurrence (Li et al., 2020).

The basic principle of fuzzy logic is the use of membership degrees in which values between 0 and 1 are provided for several fuzzy sets. Via fuzzy logic, the information of different types of parameters can be combined to describe a condition defined by any number of

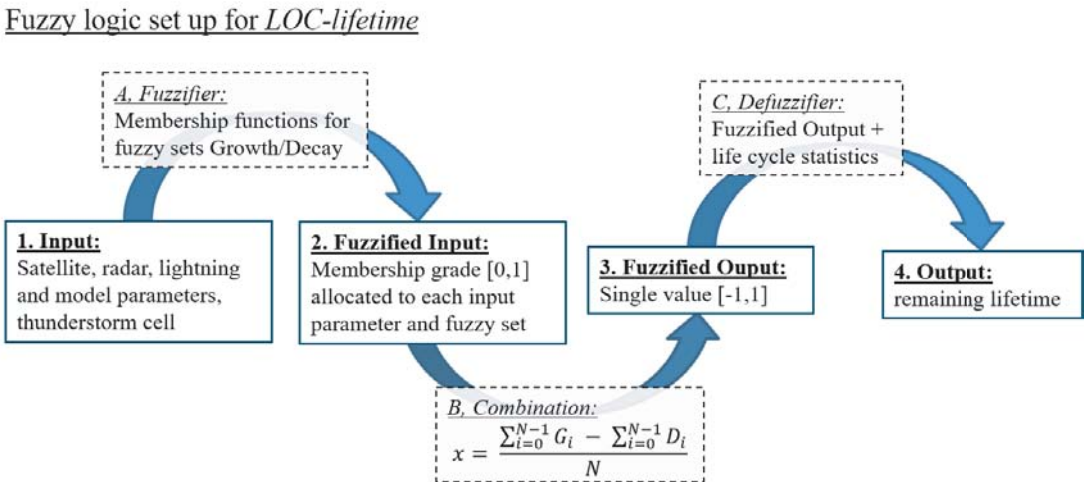

Figure 3: Scheme of the fuzzy-logic-based lifetime nowcasting algorithm LOC-lifetime.

fuzzy sets. In Figure 3, the scheme of LOC-lifetime is illustrated. The method is described step by step by the nowcasting of the thunderstorm cell over the Breisgau region (shown in Figure 1).

4.1 Input

The parameters in Table 1 provide the input set for LOC-lifetime. At the first detection step, only absolute values 'a' are used. From the second detection step on, all parameters (absolute values 'a' as well as temporal variations 't') are taken into account.

4.2 Fuzzified input

Via fuzzy logic, we categorize the development stage into two fuzzy sets describing the life cycle stages: *growth* and *decay*. The parameters are assigned to the fuzzy sets with values between 0 and 1 (membership degree). The transition area between *growth* and *decay* is comparable to the life-cycle stage *maturity* where thunderstorm growth stops and the decay process has not started yet. The membership degree is calculated via membership functions. The thresholds of the membership functions are determined as described before in Zöbisch et al. (2020).

The membership functions convert the parameter values (input set) into a fuzzified input. Now, values inside the interval $[0, 1]$ are assigned to the fuzzy sets *growth* and *decay* for every parameter.

In Figure 4, the temporal evolution (black line) of each parameter of Table 1 is shown with its corresponding calculated fuzzy input values for the fuzzy sets *growth* (dashed, blue) and *decay* (solid, red) for cell "1315" presented in Figure 1. A smoothing function is used (mean of two consecutive time steps) to reduce noise and to focus on the dominant signatures describing the life cycle stages.

General features of the early thunderstorm case over Breisgau can be noted: Three parameters (ΔA_{cb}, VIL_{max}, ΔVIL_{max}) reveal a "growth-mature-growth-mature-decay" cycle. Two parameters (BT_{min}, ΔBT_{min}) emphasize initial growth and the final decay. The temporal development of ΔLi shows a clear growth at the beginning of the second half of the life cycle and a decay at end of the life cycle. A clear growth is also revealed in $\Delta\tau_{min}$ during the first half of the life cycle, followed by alternating decay and growth phases. The parameter $CAPE_{max}$ shows decay during the whole life cycle (red line/*decay* equals 1 and blue line/*growth* equals 0) and is in this case of limited use. To detect growth, a value of 750 J/kg or higher is necessary as shown for long-lived thunderstorms in Zöbisch et al. (2020). Finally, *RH* indicates initial decay and final growth.

In the early first half of the life cycle, the thunderstorm grows vertically (seen in a decreasing BT_{min}). At the beginning, the cloud top is already relatively high at around 8 km (240 K). Some lightning activity is detected and VIL_{max} values are relatively high leading to the assumption that the early convection stage has been missed. The increasing A_{cb}, τ_{min} and VIL_{max} in addition to the decreasing BT_{min} at the beginning of the life cycle indicate an intensively growing thunderstorm.

In the late first half around 12:55, we identify signatures of reduced growth compared to the early life cycle in six parameters, becoming more indifferent and therefore indicating a mature stage and partly containing characteristics of a decaying thunderstorm. The cloud top reaches low temperatures (low BT_{min} values), starts to sink slightly (positive ΔBT_{min} values) and grows again shortly afterwards. Additionally, the horizontal extent (A_{cb}), τ_{min} values and VIL_{max} values are decreasing. The absolute values of VIL_{max} are lower compared to the early life cycle. The lightning activity ΔLi reveals still alternating characteristics of growth and decay as already seen for the early life cycle.

In the early second half of the life cycle (after 13:03), vertical growth stops as BT_{min} stagnates at 12:58 UTC. This is the time when Cb-TRAM detects maturity stage. Five parameters indicate a second growing phase.

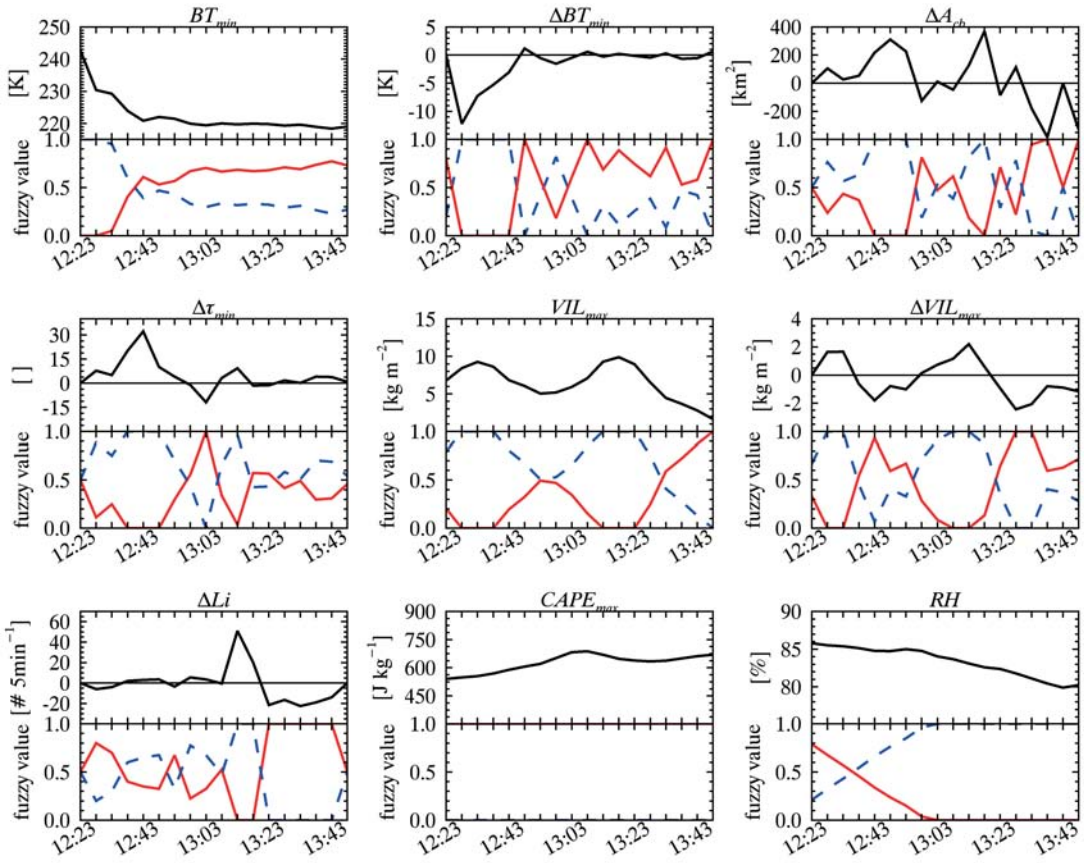

Figure 4: Temporal course of the parameters averaged over two time steps as (black) used in lifetime nowcasting with LOC-lifetime and corresponding fuzzy functions for fuzzy sets *growth* (blue, dashed) and *decay* (red, solid) for the thunderstorm case over the Breisgau region (in UTC) in Figure 1.

The $\Delta VIL_{\max}$ values as well as $\Delta\tau_{\min}$ values are again increasing. At around 13:13 UTC, Li, A_{cb} and $VIL_{\max}$ reach their maximum. Leading to the assumption that the thunderstorm reaches its maximum intensity at the beginning of the second half of the detected life cycle.

In the late second half, the life cycle is dominated by a decrease in Li, $VIL_{\max}$ and A_{cb} indicating a decaying thunderstorm cell.

4.3 Fuzzified output

The fuzzy-logic input, that is calculated for every parameter and fuzzy set, is combined to one fuzzy output value. This combination is done by (see Figure 3 step B)

$$x = \frac{\sum_{i=0}^{N-1} G_i - \sum_{i=0}^{N-1} D_i}{N} \tag{4.1}$$

where the difference of the average of each fuzzy set (G, *growth* and D, *decay*) is calculated and divided by the number of parameters N. The result is a single value, referred to as fuzzy output, inside the interval of $[-1, 1]$ indicating whether a thunderstorm is more likely to grow $(0, 1]$ or to decay $[-1, 0)$.

Figure 5 (top) displays the fuzzy output for the case study which is calculated for every detection step. In general, the fuzzy output value decreases as the life cycle progresses but we can again identify a "growth-mature-growth-mature-decay" cycle as was already dominating in the single parameters in Figure 4.

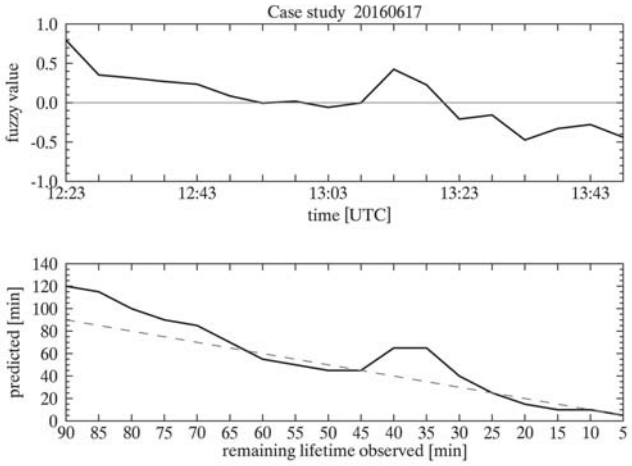

Figure 5: Top: Fuzzy values calculated via LOC-lifetime for every detection step for the thunderstorm over the Breisgau region. Bottom: The remaining lifetimes predicted with LOC-lifetime for the thunderstorm over the Breisgau region with the corresponding observed remaining lifetimes. A perfect prediction is illustrated by the dashed line.

4.4 Output

We use life cycle statistics of a large data set to defuzzify the fuzzified output to obtain the remaining lifetime. We compare the calculated fuzzy output value to the life cycle statistics that include averaged fuzzy output values for various remaining lifetimes and detection steps and generate the lifetime prediction.

For example, the fuzzy output value of the thunderstorm of the case study is approx. 0.38 at 12:28 UTC. Additionally to the fuzzy output value, we have the information that the thunderstorm has been detected for one time step. To determine the remaining lifetime of the thunderstorm, we compare this fuzzy output value to the average values of the life cycle statistics for thunderstorms that were predicted for one time step. In this case, a fuzzy output value of 0.38 at a detection step of 5 min is closest to the average fuzzy output value of thunderstorms with a total lifetime of 120 min. As the thunderstorm already has been detected for 5 min, the predicted remaining lifetime is 115 min.

In Figure 5 (bottom), the remaining lifetime is shown for every detection step for the thunderstorm case over the Breisgau region. In general, the predicted remaining lifetime (solid line) decreases during the life cycle except for observed remaining lifetimes between 45 and 35 min. As expected, the relatively high fuzzy output values during this period (as seen in Figure 5, top) are leading to a prediction of remaining lifetimes higher than observed. We see a very good correlation of observed (grey dashed line) and predicted remaining lifetimes for observed remaining lifetimes between 60–45 min and 25–5 min.

5 Verification

5.1 One dimensional lifetime frequency distribution

In this section all thunderstorm cases of the analyzed period are used to derive skill values for LOC-lifetime. No other lifetime nowcasting of thunderstorms exists so far, therefore, the reference model RNDM (random lifetime nowcasting based on lifetime frequency statistics) as a fair orientation to rate any improvement introduced by LOC-lifetime is designed. This simpler straight forward nowcasting method randomly predicts the remaining lifetime based on the lifetime frequency statistics of thunderstorms for the analyzed period. That means, for each detected case a random remaining total lifetime is picked from the real observed lifetime distribution. This guarantees that the RNDM prediction is limited to the climatology of real lifetimes.

In total, 75 thunderstorm days were counted during the five summer months including 1,758 thunderstorms and 16,288 detection steps. In Figure 6, the frequency distributions of the lifetimes of all thunderstorm cases are depicted by LOC-lifetime prediction (blue), RNDM prediction (light blue) and the observation (grey). It is obvious that all three data sets (LOC-lifetime, RNDM and observed) share the same overall distribution. On a closer inspection it can be seen, that the observed frequency decays monotonously with the remaining lifetime, while a non-monotonous behaviour can be noticed for both prediction methods. We find a slight underestimation for short and medium remaining lifetimes (< 60 min) and an overestimation for long remaining lifetimes (> 60 min) in the LOC-lifetime algorithm compared to the observation.

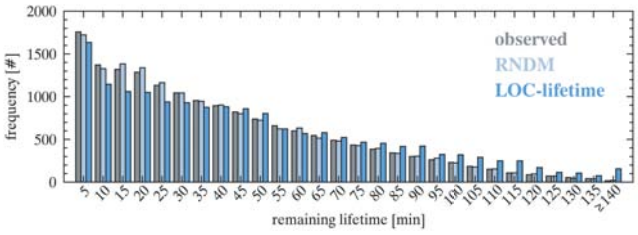

Figure 6: Frequency distribution of observed remaining lifetimes (grey), remaining lifetimes predicted with RNDM (light blue) and predicted with LOC-lifetime (blue) for thunderstorms that occurred during the analyzed period (June 2016, May, June and July 2017 and June 2018).

This is due to the fact that single months contain different mean fuzzy-logic values. For instance, an overestimation of very long lifetimes occurs due to predictions of thunderstorms in June, July 2017 and June 2018 (not shown). As life-cycle statistics used for the nowcasting of these months include data from June 2016 and May 2017 that contain lower fuzzy-logic values than average, long lifetimes (relatively high fuzzy values) are predicted more often for thunderstorms in these months. We assume that a larger data set would help to calculate life-cycle statistics more equal to the climatological mean as the influence of a single month is reduced.

On average, LOC-lifetime-predicted lifetimes are more often longer than observed (52.4 %) resulting in a longer average mean lifetime of 47 min compared to observed 41 min.

5.2 Contingency table

The nowcasting is validated via cross validation. This is done to guarantee independent data sets, as data of the month to be nowcasted are excluded for the calculation of the life cycle statistics. This is done for each month. Hence, for example, the fuzzy output values of the case study in June 2016 are compared to life cycle statistics of thunderstorms that occurred in May, June, July 2017 and June 2018. The validation contains predictions of every detection step for thunderstorms detected during the analyzed period.

We use contingency tables to calculate verification indices for LOC-lifetime and RNDM. The probability

Table 2: POD values of LOC-lifetime and RNDM for different exemplary sizes of tolerance intervals [min].

tolerance interval [min]	**0**	**±5**	**±10**	**±15**	**±20**	**±25**	**±30**	**±35**	**±40**	**±45**
POD LOC-lifetime	9.2	22.9	35.0	45.5	54.2	61.8	68.5	74.2	79.0	83.3
POD RNDM	5.9	16.7	26.6	35.7	43.7	50.8	57.1	63.5	68.9	73.5

of detection

$$POD = \frac{hits}{hits + misses} \tag{5.1}$$

is used to determine the ratio of the correct prediction. The perfect score is 1.

We calculate the false alarm ration

$$FAR = \frac{false\ alarms}{hits + false\ alarms} \tag{5.2}$$

to determine the amount of false predictions. It is calculated by means of false alarms and hits. The perfect score is 0. In contrast to a miss (where missed observed remaining lifetimes are relevant), the incorrect predicted remaining lifetimes are considered in the false alarms. For instance, if LOC-lifetime predicts 90 min for an observed remaining lifetime of 65 min, a miss is assigned to 65 min and a false alarm to 90 min.

To determine general overestimation (>1) or underestimation (<1) of the remaining lifetimes the BIAS

$$BIAS = \frac{hits + false\ alarms}{hits + misses} \tag{5.3}$$

is calculated. The perfect score is 1.

We calculate the root mean squared error to determine the distance between observed remaining lifetime (O) and predicted remaining lifetime (P)

$$RMSE = \frac{\sum_{i=1}^{N}(P_i - O_i)^2}{N} \tag{5.4}$$

as a measure of quality. The perfect score is 0.

A reliable prediction to the minute is hard to achieve with respect to the high variable life cycles. However, depending on the application of the nowcasting, a prediction to the minute is not indispensable and a prediction range is tolerable. We calculated POD values for various tolerance intervals. In Table 2, tolerance intervals from 0 to 45 min were used to calculate POD values of LOC-lifetime and RNDM. As expected, the POD values increase with an increasing tolerance interval. Additionally, we can identify that the POD of LOC-lifetime is higher than the POD of RNDM, regardless of the size of the tolerance interval. Especially for small tolerance intervals, we see a relatively high increase of POD. The trade-off between tolerable prediction range and POD values depends on the individual nowcasting application. In the following analyses, we use a tolerance interval of ±10 min as this tolerance interval shows a comparatively strong increase in POD while the predictions counted as correct are still in temporal vicinity to the real remaining lifetime.

If we use one contingency table for all lifetime predictions, LOC-lifetime shows higher skill in quality (POD = 35.0, RMSE = 34.9) than RNDM (POD = 26.6, RMSE = 42.5); note that FAR − 1 equals POD as every false alarm is counted as miss for the observed lifetime. The prediction-quality measures POD, FAR, RMSE and BIAS, calculated for each lifetime separately, are shown in Figure 7 for LOC-lifetime and RNDM predictions. The variability from thunderstorm to thunderstorm is reflected in the shaded area (minimum and maximum values of the individual months).

In general, we identify a gain in nowcasting quality when using the LOC-lifetime algorithm, since the POD/FAR values are higher/lower for all lifetimes compared to RNDM predictions. Both methods reveal similar signatures in POD and FAR: POD first increases for lifetimes up to 15 min and decrease for lifetimes beyond 15 min. FAR shows the inverse signature. The increase of quality for lifetimes between 5–15 min is caused by the tolerance interval of 10 min.

The BIAS values confirm the findings from Figure 6: short lifetimes up to 45 min are underestimated (BIAS <1) whereas lifetimes longer than 70 min are overestimated in LOC-lifetime (BIAS >1). Please note that we excluded the BIAS value for lifetimes of 140 min and more as it is of limited use due to the accumulation effect. As RNDM predictions are based on the lifetime frequency statistics of the observed remaining lifetimes, its BIAS is near 1 for all lifetimes.

The RMSE values of LOC-lifetime predictions are relatively constant for lifetimes up to 70 min but increase afterwards. RMSE values of RNDM predictions show a decrease first until lifetimes of 40 min and then also increase. This minimum around 40 min reflects the average lifetime of RNDM predictions of around 41 min. On the other hand, the relatively constant RMSE values for lifetimes between 5–70 min for LOC-lifetime predictions reflect the increase in quality gained with the LOC-lifetime algorithm. In summary, for all lifetimes, LOC-lifetime predictions show RMSE values equal to or lower than those of RNDM predictions.

5.3 Two-dimensional lifetime-frequency distribution

A more detailed view on the lifetime-frequency distribution is provided when a predicted lifetime is compared to the observed remaining lifetime separately for every detection step, leading to a two-dimensional lifetime-frequency distribution of Figure 8. It shows the predicted remaining lifetimes (rows) with the corresponding observed remaining lifetimes (columns) relative to the frequency of each observed remaining lifetime (row at the

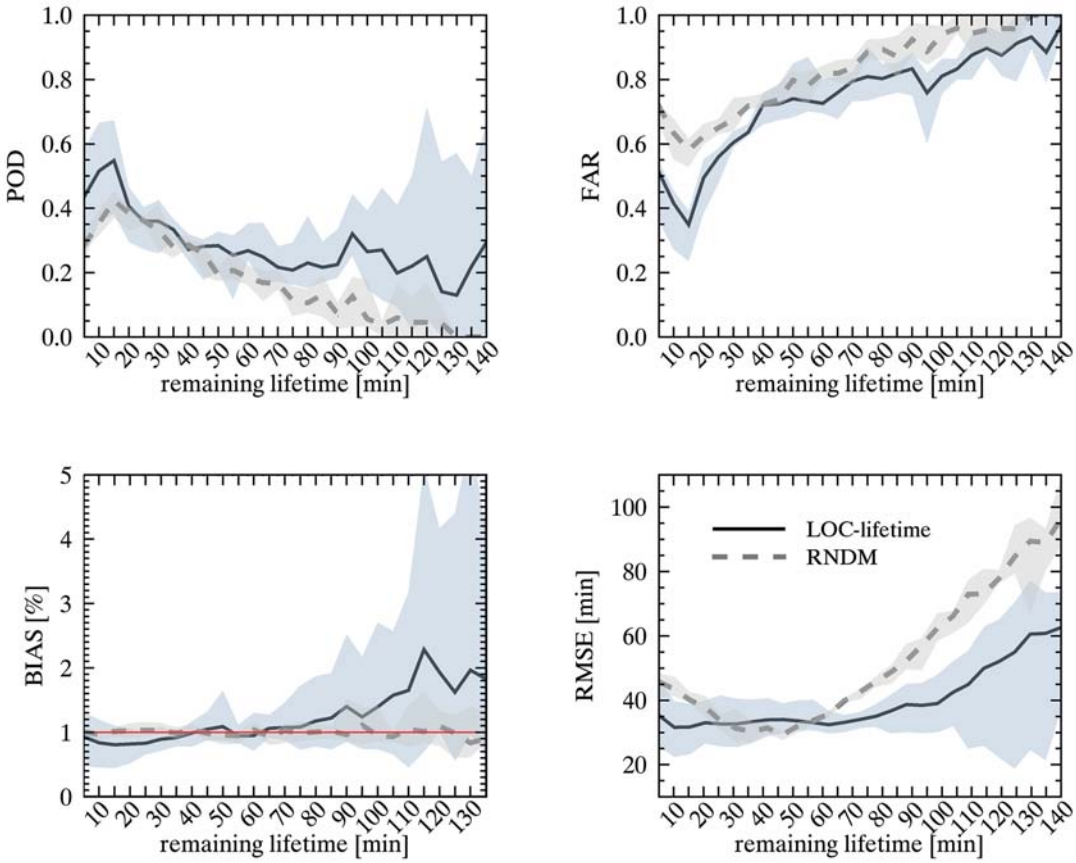

Figure 7: Prediction verification indices POD, FAR, BIAS and RMSE for LOC-lifetime (black solid line) and RNDM (grey dashed line) for a tolerance interval of ±10 minutes. Minimum and maximum values of the indices for the single months are represented by the shaded areas.

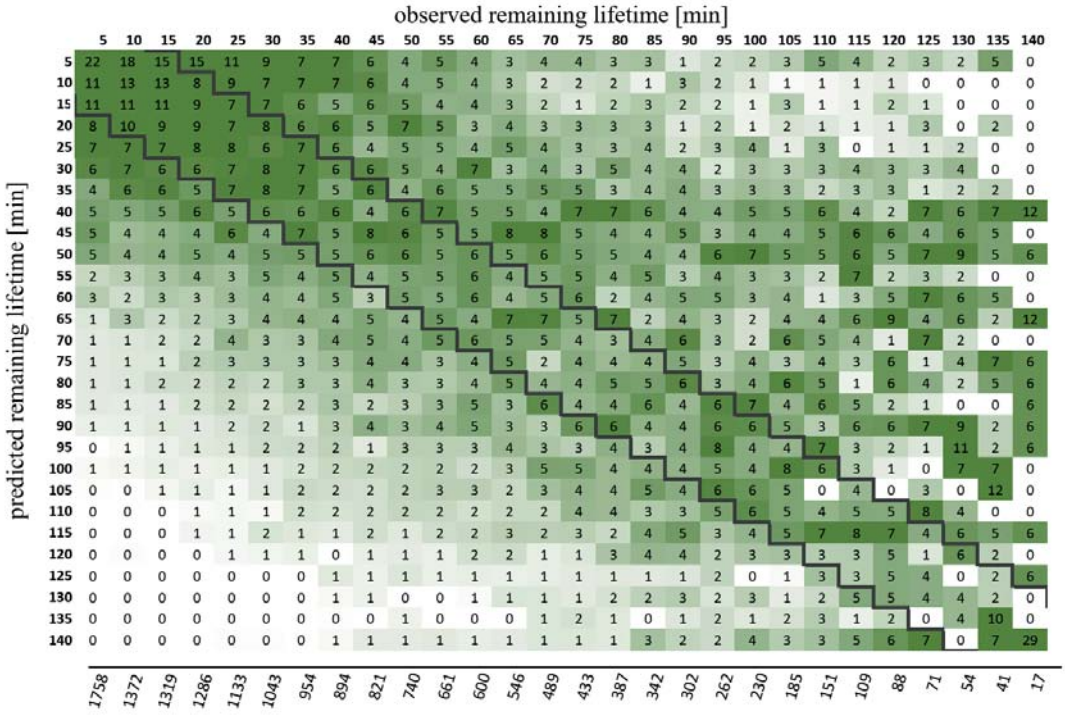

Figure 8: Remaining lifetimes predicted with LOC-lifetime (rows) with the corresponding observed remaining lifetimes (columns) relative to the frequency of each observed remaining lifetime (row at the bottom of the figure). The area inside the dark gray borders represents the tolerance interval of ±10 min.

bottom of the figure). Thus, the sum of each column equals 100 and we can estimate the frequency distribution independently of the absolute number of remaining lifetimes. The intensity of the color indicates the value of the relative number of thunderstorms. In the case of only correct predictions, we would see deep green cells inside the gray borders (which represent the tolerance interval of ±10 min) running diagonally from the top left to the bottom right corner.

For example, we now can identify that 5 % of thunderstorms with an observed remaining lifetime of 95 min are predicted to have a remaining lifetime of 100 min. As 262 thunderstorms were analyzed with an observed remaining lifetime of 95 min, this corresponds to a number of 13 thunderstorms. The figure also reveals the POD values as presented in Figure 7, as they can be obtained by a column-wise accumulation of the values inside the grey borders. For instance, observed remaining lifetimes of 95 min show a POD value of 31 % (6 + 6 + 8 + 5 + 6) for a tolerance interval of ±10 min.

Short observed remaining lifetimes (up to 40 min) are predicted mainly as short remaining lifetimes (deep green cells in the upper left corner). However, we also see slightly shorter and longer predicted remaining lifetimes since deep green cells are found outside but close to the borders. As the colors in the columns fade from short predicted remaining lifetimes (top) to long predicted remaining lifetimes (bottom), we can conclude that for observed short remaining lifetimes, longer predicted remaining lifetimes are less frequent although they do occur.

Medium observed remaining lifetimes (approx. between 40 and 90 min) are mostly predicted as medium and short-to-medium remaining lifetimes (area above the diagonal). The decreased nowcasting quality can be seen in a colored diagonal that becomes fuzzier and widespread for medium lifetimes. As for the short observed remaining lifetimes, we can again identify a reduced frequency for longer predicted lifetimes. This pattern can also be identified for much shorter predicted lifetimes (< 40 min). Thus, shorter lifetimes are predicted less frequently.

Long observed remaining lifetimes are predicted as short-to-medium, medium and long remaining lifetimes (approx. between 40 and 140 min). The diagonal is now even more fuzzy as predicted remaining lifetimes become more inaccurate for long observed lifetimes. Very short remaining lifetimes are predicted rarely.

In general, the figure enables a more detailed view than RMSE analysis on the remaining lifetime frequency distribution, which is especially valuable to analyze incorrectly predicted remaining lifetimes.

6 Conclusion

We present a new algorithm, named LOC-lifetime, to predict the lifetime of detected thunderstorm cells based on life-cycle information of a large number of thunderstorms. We use a fuzzy-logic approach to combine data from satellite, radar, lightning and NWP model during five summer months. In order to assess the features and quality of LOC-lifetime, we compare its output to the output of a simpler, climatologically correct random choice approach RNDM, where the remaining lifetimes are predicted based on the lifetime frequency statistics of the thunderstorms in the analyzed period.

The analysis reveals that the average remaining lifetime predicted via LOC-lifetime is 47 min. This is 6 min longer than the observed time of 41 min. The overprediction is also reflected in the tendency of LOC-lifetime to predict longer lifetimes (52.4 %) more frequently than shorter lifetimes (38.5 %) compared to the observed remaining lifetimes. On the other hand, we see a gain in nowcasting quality in terms of a reduction of RMSE of about 17.8 %, an increase in POD of about 31.6 % and a decrease in FAR of about 11.4 %, compared to the RNDM approach in case a tolerance interval of ±10 min is used. In general, we identify a gain in nowcasting quality when using the LOC-lifetime algorithm, but these improvements are relatively modest. This could be expected as the prediction of thunderstorms is a well-known challenge due to complex interactions of dynamics and microphysics during their lifetime, reflected, for example, in the different types of organization.

We do not distinguish between the different organization types of thunderstorms (e.g., single cells or multi cells) since our aim is an automated nowcasting of thunderstorms and no automated method to separate these types is available yet. However, as the most frequent type of development are multi-cell thunderstorm systems, events like splitting and merging lead to high variability between single life cycles and the corresponding fuzzy values.

Since these life cycles build the basis for the life cycle statistics used for prediction, they affect nowcasting of the remaining lifetime. Potential improvements could be achieved via a larger data set to obtain an average life cycle that is closer to the actual climatological mean as well as via a modification of the fuzzy logic set up. A possible improvement could be achieved when using individual weights for the different data sources, regarding their relevance. First analyses showed that especially satellite and radar data are relevant for the lifetime nowcasting of LOC-lifetime. However a detailed analysis is planned. These preliminary results are in coincidence with existing studies as, for instance, Leinonen et al. (2021) who analyzed the influence of satellite, radar, lightning and NWP model data to the quality of thunderstorm nowcasting in a machine learning based approach. They showed that especially radar as well as satellite parameters are relevant for the nowcasting. It can be anticipated that the quality of LOC-lifetime predictions can be improved by adding different weighting functions to the fuzzy logic set. More suitable thresholds and weighting functions could be identified, e.g., via machine learning.

We defined a thunderstorm here as a detection by the satellite based algorithm Cb-TRAM. Other thun-

derstorm definitions based on other automatic detection algorithms as for example, Rad-TRAM are not tested. However, we assume that the nowcasting can be used in combination with other detection algorithms than Cb-TRAM since the nowcasting is based on physical characteristics valid generally for thunderstorm evolution.

Last but not least, the algorithm can be combined with algorithms to forecast thunderstorms beyond the nowcasting scale as, for example, Cb-fusion (Li et al., 2020), where observed thunderstorm objects are forecast up to 6 h on basis of observational and NWP data. The predicted remaining lifetime from LOC-lifetime can be used as an additional ingredient to calculate the future thunderstorm likelihood during the next two hours.

Acknowledgement

We want to thank Caroline Reitwiesner and Thomas Gerz for helpful discussions and their valuable feedback. We also want to thank Caroline for providing Cb-TRAM data and Luca Bugliaro for providing APICS and COCS data. We are grateful to the nowcast GmbH for providing the lightning data, to the German Meteorological Service for providing Radar and NWP data, and to EUMETSAT for providing the Meteosat data. Meteosat data are copyrighted by EUMETSAT.

Acronyms

A_{cb}	Area of the Cb-TRAM cell
BT	Brightness Temperature
BT_{min}	minimum Brightness Temperature
CAPE	Convective Available Potential Energy
$CAPE_{max}$	maximum Convective Available Potential Energy
Cb-TRAM	Cumulonimbus Tracking And Monitoring
HRV	High Resolution Visible channel
IR	Infra-Red channel
Li	Lightning detection during 5 min
LINET	European ground-based Lightning Network
NWP	Numerical Weather Prediction
O	observed remaining lifetime
P	predicted remaining lifetime
RH	Relative Humidity at 700 hPa
SEVIRI	Spinning Enhanced Visible and Infra-Red Imager
τ	cloud optical thickness
τ_{min}	minimum cloud optical thickness
VIL	Vertically Integrated Liquid water
VIL_{max}	maximum Vertically Integrated Liquid water
VIS	Visible channel
WV	Water Vapor channel

References

Baldauf, M., K. Stephan, S. Klink, C. Schraff, A. Seifert, J. Förstner, T. Reinhardt, C.J. Lenz, 2006: The new very short range forecast model LMK for the convection-resolving scale. – Second THORPEX International Science Symposium **Volume of extended abstracts Part B**, 148–149.

Betz, H.D., K. Schmidt, P. Laroche, P. Blanchet, W.P. Oettinger, E. Defer, Z. Dziewit, J. Konarski, 2009: LINET – An international lightning detection network in Europe. – Atmos. Res. **91**, 564–573, DOI: 10.1016/j.atmosres.2008.06.012.

Brooks, H., N. Dotzek, 2008: The spatial distribution of severe convective storms and an analysis of their secular changes. – Climate Extremes and Society, Cambridge University Press, DOI: 10.1017/CBO9780511535840.

Bugliaro, L., T. Zinner, C. Keil, B. Mayer, R. Hollmann, M. Reuter, W. Thomas, 2011: Validation of cloud property retrievals with simulated satellite radiances: a case study for SEVIRI. – Atmos. Chem. Phys. **11**, 5606–5624, DOI: 10.5194/acp-11-5603-2011.

Byers, H.R., R.R. Braham Jr., 1948: Thunderstorm structure and circulation. – J. Meteor. **5**, 71–86, DOI: 10.1175/1520-0469(1948)005<0071:TSAC>2.0.CO;2.

Cintineo, R.M., M.J. Pavolonis, J.M. Sieglaff, D.T. Lindsey, G.L. Cronce, B.B. Rodenkirch, C. Gravelle, 2018: The NOAA/CIMS ProbSevere model: Incorporation of total lightning and validation. – Wea. Forecast. **33**, 331–345, DOI: 10.1175/WAF-D-17-0099-1.

Davini, P., R. Bechini, R. Cremonini, C. Cassardo, 2012: Radar-based analysis of convective storms over northwestern Italy. – Atmosphere **3**, 33–58, DOI: 10.3390/atmos3010033.

Feng, Z., X. dong, B. Xi, S.A. McFarlane, A. Kennedy, B. Ling, P. Minnis, 2012: Life cycle of midlatitude deep convective systems in a Lagrangian framework. – J. Geophys. Res. **117**, DOI: 10.1029/2012JD018362.

Forster, C., A. Ritter, S. Gemsa, A. Tafferner, D. Stich, 2016: Satellite-Based Real-Time Thunderstorm Nowcasting for Strategic Flight Planning En Route. – J. Air Transport. **24**, 113–124, DOI: 10.2514/1.D0055.

Goyal, S., A. Kumar, M. Mohapatra, L.S. Rathore, S.K. Dube, R. Saxena, R.K. Giri, 2017: Satellite-based technique for nowcasting of thunderstorms over indian region. – J. Earth Syst. Sci. **126**, 79.

Greene, D.R., R.A. Clark, 1972: Vertically integrated liquid water – A new analysis tool. – Mon. Wea. Rev. **100**, 548–552.

Hansen, B.K., 1997: SIGMAR: a fuzzy expert system for critiquing marin forecasts. – AI Appl. **11**, 59–68.

Hansen, B.K., 2007: A Fuzzy Logic-Based Analog Forecasting System for Ceiling and Visibility. – Wea. Forecast. **22**,1319–1330 DOI: 10.1175/2007WAF2006017.1.

Hering, A., G. Nisi, D. Bruna, M. Gaia, D. Nerini, P. Ambrosetti, U. Hamann, S. Trefalt, U. Germann, 2015: Fully automated thunderstorm warnings and operational nowcasting at MeteoSwiss. – Proc. of European Conference on Severe Storms, Wiener Neustadt, Austria.

Hertl, S., G. Schaffar, 1998: An autonomous approach to road temperature prediction. – Meteor. Appl. **5**, 227–238, DOI: 10.1017/S1350482798000838.

James, P.M., B.K. Reichert, D. Heizenreder, 2018: NowCastMIX: Automatic integrated warnings for severe convection on nowcasting time scales at the German Weather Service. – Wea. Forecast. **3**, 413–433, DOI: 10.1175/WAF-D-18-0038.1.

Jurković, P.M., N.S. Mahović, D. Počakal, 2015: Lightning, overshooting top and hail characteristics for strong convective storms in Central Europe. – Atmos. Res. **161-162**, 153–168, http://www.sciencedirect.com/science/article/pii/S0169809515001155.

Kahraman, A., M. Kadiglu, P. Markowski, 2017: Severe convective storm environments in Turkey. – Mon. Wea. Rev. **145**, 4711–4725, DOI: 10.1175/MWR-D-16-0338.1.

Kaltenböck, R., G. Diendorfer, N. Dotzek, 2009: Evalutation of thunderstorm indices from ECMWF analyses, lightning data and severe storm reports. – Atmos. Res. **93**, 381–396, DOI: 10.1016/j.atmosres.2008.11.005.

Kober, K., A. Tafferner, 2009: Tracking and nowcasting of convective cells using remote sensing data from radar and satellite. – Meteorol. Z. **18**, 75–84, DOI: 10.1127/0941-2948/2009/359.

Kox, S., L. Bugliaro, A. Ostler, 2014: Retrieval of cirrus cloud optical thickness and top altitude from geosationary remote sensing. – Atmos. Measur. Techniques **7**, 3233–3246, DOI: 10.5194/amt-7-3233-2014.

Kuligowski, R.J., A.P. Barros, 1998: Localized precipitation forecasts from a numerical weather prediction model using artifical neural networks. – Wea. Forecast. **13**, 1194–1204, DOI: 10.1175/1520-0434(1998)013<1194:LPFFAN>2.0.CO;2.

Leinonen, J., U. Hamann, U. Germann, J.R. Mecikalski, 2021: Nowcasting thunderstorm hazards using machine learning: the impact of data sources on performance. – Nat. Hazards Earth Sys. Sci. Discuss. **2021**, 1–28, DOI: 10.5194/nhess-2021-171.

Leinonen, J., U. Hamann, I.V. Sideris, U. Germann, 2022: Thunderstorm nowcasting with deep learning: a multi-hazard data fusion model. – arXiv preprint arXiv:2211.01001, DOI: 10.48550/arXiv.2211.01001.

Li, J., C. Forster, J. Wagner, T. Gerz, 2020: Cb-Fusion – forecasting thunderstorm cells up to 6 hours. – Meteorol. Z. **30**, 169–184, DOI: 10.1127/metz/2020/1047.

Machado, L.A.T., W.B. Rossow, R.L. Guedes, A.W. Walker, 1997: Life cycle variations of mesoscale convective systems over the Americas. – Mon. Wea. Rev. **126**, 1630–1654, DOI: 10.1175/1520-0493(1998)126<1630:LCVOMC>2.0.CO;2.

Mathon, V., H. Laurent, 2001: Life cycle of Sahelian mesoscale convective cloud systems. – Quart. J. Roy. Meteor. Soc. **127**, 377–406, DOI: 10.1002/qj.49712757208.

Mattos, E.V., L.A.T. Machado, 2011: Cloud-to-ground lightning and mesoscale convective systems. – Atmos. Res. **99**, 377–390 DOI: 10.1016/j.atmosres.2010.11.007.

Mecikalski, J., P.D. Watts, M. König, 2011: Use of Meteosat Second Generation optimal cloud analysis field for understanding physical attributes of growing cumulus clouds. – Atmos. Res. **102**, 175–190, DOI: 10.1016/j.atmosres.2011.06.023.

Mueller, C., T. Saxen, R. Roberts, J. Wilson, T. Betancourt, S. Dettling, N. Oien, J. Yee, 2003: NCAR Auto-Nowcast System. – Wea. Forecast. **18**, 545–561, DOI: 10.1175/1520-0434(2003)018<0545:NAS>2.0.CO;2.

Rädler, A.T., P.H. Groenemeijer, E. Faust, R. Sausen, T. Púčik, 2019: Frequency of severe thunderstorms across Europe expected to increase in the 21st century due to rising instability. – Climate Atmos. Sci. **2**, DOI: 10.1038/s41612-019-0083-7.

Rigo, T., N. Pineda, J. Bech, 2010: Analysis of warm season thunderstorms using an object-oriented tracking method based on radar and total lightning data. – Nat. Hazards Earth Sys. Sci. **10**, 1881–1893 10.5194/nhess-10-1881-201.

Roberts, R.D., S. Rutledge, 2003: Nowcasting storm initiation and growth using GOES-8 and WSR-88D data. – Wea. Forecast. **18**, 562–584, DOI: 10.1175/1520-0434(2003)018<0562:NSIAGU>2.0.CO;2.

Sander, J., 2011: Extremwetterereignisse im Klimawandel: Bewertung der derzeitigen und zukünftigen Gefährdung. – Faculty of Physics, Disseration, LMU München, 125 pp.

Schmetz, J., P. Pili, S. Tjemkes, D. Just, J. Kerkmann, S. Rota, A. Ratier, 2002: An introduction to Meteosat Second Generation (MSG). – Bull. Amer. Meteor. Soc. **83**, 977–992, DOI: 10.1175/1520-0477(2002)083<0977:AITMSG>2.3.CO;2.

Stich, D., 2013: Convection initiation. – Faculty of Physics, Disseration, LMU München, https://nbn-resolving.org/urn:nbn:de:bvb:19-157194.

Tafferner, A., C. Forster, M. Hagen, C. Keil, T. Zinner, H. Volkert, 2008: Development and propagation of severe thunderstorms in the Upper aube catchment area: Towards an integrated nowcasting and forecasting system using real-time data and high-resolution simulations. – Meteor. Atmos. Phys. **101**, 211–227, DOI: 10.1007/s00703-008-0322-7.

Wapler, K., 2021: Mesocyclonic and non-mesocyclonic convective storms in Germany: Storm characteristics and life-cycle. – Atmos. Res. **248**, 10.1016/j.atmosres.2020.105186.

Wilson, J.W., N.A. Crook, C.K. Mueller, J. Sun, M. Dixon, 1998: Nowcasting thunderstorms: A status report. – Bull. Amer. Meteor. Soc. **79**, 2079–2099, DOI: 10.1175/1520-0477(1998)079<2079:NTASR>2.0.CO;2.

Zadeh, L.A., 1965: Fuzzy sets. – Information control **8**, 338–353, DOI: 10.1016/S0019-9958(65)90241-X.

Zinner, T., H. Mannstein, A. Tafferner, 2008: Cb-TRAM: Tracking and monitoring severe convection from onset over rapid development to mature phase using multi-channel Meteosat-8 SEVIRI data. – Meteor. Atmos. Phys. **101**, 191–210, DOI: 10.1007/s00703-008-0290-y.

Zinner, T., C. Forster, E. de Coning, H.D. Betz, 2013: Validation of Meteosat storm detection and nowcasting system Cb-TRAM with lightning network data – Europe and South Africa. – Atmos. Measur. Techn. **6**, 1567–1585, DOI: 10.5194/amt-6-1567-2013.

Zöbisch, I., C. Forster, T. Zinner, L. Bugliaro, A. Tafferner, K. Wapler, 2020: Characteristics of deep moist convection over Germany in multi-source data. – Meteorol. Z. **29**, 393–407, DOI: 10.1127/metz/2020/1011.